

Orthorhombic Yb:Li₂Zn₂(MoO₄)₃ – A novel potential crystal for broadly tunable lasers

Sergei Kurilchik,^{1,2} Pavel Loiko,^{3,*} Anatol Yasukevich,¹ Vyacheslav Trifonov,⁴ Anna Volokitina,³ Elena Vilejshikova,¹ Viktor Kisel,¹ Xavier Mateos,⁵ Alexander Baranov,³ Oleg Goriev,² Nikolay Kuleshov¹ and Anatoly Pavlyuk⁴

¹Center for Optical Materials and Technologies (COMT), Belarusian National Technical University, 65/17 Nezavisimosti Ave., 220013 Minsk, Belarus

²Kazan Federal University, 18 Kremlevskaya St., 420008 Kazan, Russia

³ITMO University, 49 Kronverkskiy pr., 197101 St. Petersburg, Russia

⁴A. V. Nikolaev Institute of Inorganic Chemistry, Siberian Branch of Russian Academy of Sciences, 3 Lavrentyev Ave., 630090 Novosibirsk, Russia

⁵Física i Cristal·lografia de Materials i Nanomaterials (FiCMA-FiCNA), Universitat Rovira i Virgili (URV), Campus Sescelades, c/ Marcel·lí Domingo, s/n., E-43007 Tarragona, Spain

*Corresponding author: kinetic@tut.by

Abstract Crystal with composition Li₂Zn₂(MoO₄)₃ doped with 0.7 at.% Yb (Yb:LiZnMo), with high optical quality and few cm long is grown from the flux using Li₂MoO₄ as a solvent. Yb:LiZnMo is orthorhombic (sp. gr. *Pnma*, $a = 5.0843$ Å, $b = 10.4927$ Å, $c = 17.6742$ Å, $Z = 4$). Polarized Raman spectra are studied for this crystal; the most intense band is observed at 898 cm⁻¹. The absorption, stimulated-emission and gain cross-sections of Yb³⁺ ions are determined for the principal light polarizations, $E \parallel a, b, c$. The maximum $\sigma_{SE} = 6.6 \times 10^{-21}$ cm² at 1011 nm for $E \parallel b$. The gain bandwidth for Yb:LiZnMo is up to ~50 nm. The radiative lifetime of the Yb³⁺ ions is 1.55 ms. The Yb:LiZnMo crystals are very promising for broadly tunable lasers.

Keywords: molybdate crystals, ytterbium, laser materials, stimulated-emission, Raman spectra.

1. Introduction

Ytterbium (Yb^{3+}) ions are attractive for the development of efficient lasers emitting at $\sim 1 \mu\text{m}$ due to the ${}^2\text{F}_{5/2} \rightarrow {}^2\text{F}_{7/2}$ transition. They possess a simple energy-level scheme exempt of excited-state absorption (ESA) and upconversion (UC), thus leading to weak heat loading, they can be pumped at $0.94\text{-}0.98 \mu\text{m}$ by commercial and powerful InGaAs laser diodes resulting in high laser efficiency and offer a certain tuning of the laser emission wavelength. When embedded in low-symmetry [1] or disordered [2] crystals, Yb^{3+} ions can provide additional benefits arising from the broadening of their absorption and emission spectral bands. This effect is relevant, e.g., for broadly tunable [3,4] or mode-locked (ML) lasers [5-8] capable of generating sub-100 fs pulses.

Complex tungstate and molybdate crystals are well-known hosts for Yb^{3+} doping. The most prominent examples are monoclinic double tungstates (DTs), $\text{KRE}(\text{WO}_4)_2$ [1], and tetragonal scheelite-like DTs [2,9] and double molybdates [10] (DMos), $\text{ARE}(\text{XO}_4)_2$ ($\text{A} = \text{Na}$ or Li , $\text{X} = \text{W}$ or Mo), where RE^{3+} is a rare-earth element. Monoclinic DTs offer a higher Yb^{3+} doping levels possibility [11], better thermal properties [12] and stronger anisotropy of the transition cross-sections [13,14] which determine their use in power-scalable continuous-wave (CW) [15,16], passively Q-switched (PQS) [17] and especially ML lasers [5-8,18]. Tetragonal Yb^{3+} -doped DTs and DMos feature broader spectral bands due to their locally disordered structure [2,10].

Besides tetragonal DMos, there are many complex molybdates of different crystal class. For example, there exist orthorhombic lithium metal triple molybdates with chemical formula $\text{Li}_2\text{M}_2(\text{MoO}_4)_3$ (shortly LiMMo), where $\text{M}^{2+} = \text{Mg}$, Zn , Mn , Ni , or Co [19]. To date, the studies of the LiMMo single-crystals focused mostly on their possible applications as scintillators [20] and hosts for transition-metal ions, e.g. Co^{2+} [21,22]. It was shown that it is possible to grow large-volume LiMMo crystals of good optical quality. The lyonsite-type structure [19] of these materials was refined [21,23] and the elastic properties are also known [24]. Recently, the authors of [25] prepared powders of powdered $\text{Eu}:\text{LiZnMo}$ via the solid-state reaction method showing an intense red luminescence from Eu^{3+} . Later on, a LiMgMo single-crystal doped with Eu^{3+} was grown [26]. Using Eu^{3+} as a structural probe, it was argued that the rare-earth ions accommodate in a single type of site.

In the present work, we aimed to grow and study the spectroscopic properties of Yb^{3+} -doped LiZnMo single-crystal as a promising laser material, for the first time, to the best of our knowledge.

2. Crystal growth and structure

2.1 Crystal growth

The $\text{Li}_2\text{Zn}_2(\text{MoO}_4)_3$ compound melts incongruently at $885 \text{ }^\circ\text{C}$ and during the melting, it is partially decomposed: $\text{Li}_2\text{Zn}_2(\text{MoO}_4)_3 \rightarrow \text{Li}_2\text{MoO}_4 + 2\text{ZnMoO}_4$. Thus, it cannot be grown by the conventional Czochralski method. In the present work, Yb^{3+} -doped LiZnMo crystals were grown from the flux using $[010]$ -oriented ($\pm 1^\circ$) undoped LiZnMo seeds with dimensions $5 \times 5 \times 25 \text{ mm}^3$. Lithium molybdate Li_2MoO_4 was used as a solvent. The solubility C of LiZnMo in Li_2MoO_4 decreases from ~ 95 to $50 \text{ mol}\%$ with a decrease of temperature T from ~ 875 to $845 \text{ }^\circ\text{C}$ according to the equation $C = -0.0086T^2 + 1.9929T + 765.39$ (C is in $\text{mol}\%$ and T is in $^\circ\text{C}$) [27]. First, the Li_2MoO_4 solvent was prepared and then the Li_2CO_3 , ZnO , MoO_3 and Yb_2O_3 reagents (3-4N purity) were added with an excess of Li_2CO_3 and MoO_3 (5-15 $\text{mol}\%$) over the stoichiometry. The concentration of Yb^{3+} in the growth charge was 2 or 10 at.% (with respect to the Zn^{2+} content).

For the crystal growth, a Pt crucible (diameter: 70 mm, height: 120 mm) was used. It was covered by a Pt lid with a small hole. The solution ($\text{Li}_2\text{Zn}_2(\text{MoO}_4)_3 - 5\text{-}15 \text{ mol}\%$ Li_2MoO_4) was heated at $\sim 20\text{-}30 \text{ }^\circ\text{C}$ above the equilibrium temperature and homogenized with

a Pt stirrer for 1-2 h. Then, it was cooled down to 880 °C and the seed (rotating at 12 rev/min) was put in contact to the solution surface. The growth was performed under low thermal gradients (< 1 °C/cm). During the growth, the temperature was controlled and decreased for 10-15 °C with a precision of 0.1 °C, the pulling rate was 1.5-5 mm/day and the rotation speed was 10-20 rev/min. The crystallization rate was ~ 0.3 -10 g/day. The crystal weight was 150-200 g. When the growth was completed, the crystal was carefully removed from the flux and slowly cooled to room temperature (RT) at a cooling rate of 30 °C/h. No annealing of the grown crystals was applied. A photograph of the as-grown 2 at.% (nominal) Yb:LiZnMo is shown in figure 1. It was transparent, crack- and inclusion-free and had a slight brown coloration. For 10 at.% (nominal) Yb³⁺ doping, the as-grown crystal contained numerous inclusions oriented along the [100] axis.

2.2 Crystal structure

The crystal structure and phase purity of the grown Yb:LiZnMo crystals were confirmed with X-ray powder diffraction (XRD). The XRD measurements were performed using a Shimadzu XRD-6000 diffractometer, Cu K α radiation with a Ni filter. The obtained XRD pattern for the 2 at.% (nominal) Yb:LiZnMo crystal is shown in figure 2 and compared with that of the parent compound - Li₃Fe(MoO₄)₃ (ICCD card 01-072-0754) [28]. The grown Yb:LiZnMo crystals are orthorhombic (point group: *mmm*, space group: D_{2h}¹⁶ - *Pnma* (No. 62)). The determined lattice constants are $a = 5.0843$ Å, $b = 10.4927$ Å, $c = 17.6742$ Å, $Z = 4$, the unit-cell volume $V = 942.89$ Å³, and the calculated density $\rho = 4.22$ g/cm³ (for 2 at.% (nominal) Yb³⁺ doping) They are relatively close to those for undoped LiZnMo with a stoichiometric composition, $a = 5.1139$ Å, $b = 10.4926$ Å, $c = 17.645$ Å [29].

The habit of the as-grown boule of Yb:LiZnMo is schematically represented in figure 3. The bottom part of the boule is formed by the (010) pinacoid surrounded by (011) and (013) prismatic faces. The density of dislocations on the (010) plane measured after etching with 10% HCl is $\sim 4 \times 10^2$ cm⁻². The boule cross-section extends along the [100] axis. The central part of the boule is formed by the (001) pinacoids and (110) prisms.

The fragment of the LiZnMo structure in projection on the *b-c* plane is shown in figure 4. The LiZnMo crystal belongs to the vanadate mineral lyonsite Cu₃Fe₄(VO₄)₆ structural type. The Mo⁶⁺ cations occupy tetrahedral sites. The lower oxidation-state cations Li⁺, Zn²⁺ occupy three different low-symmetry sites forming chains of octahedral polyhedrons (A(1) site), face-sharing highly distorted octahedrons (A(2) site) and edge-sharing trigonal prisms (A(3) site). According to our previous study of an isostructural LiMgMo crystal doped with Eu³⁺ ions serving as a structural probe, the rare-earth dopants will replace the Zn²⁺ ions in a single type of site, A(3) [26]. This process will be accompanied by a cationic redistribution over the A sites to maintain the charge compensation. The A–O distances for the A(3) site is 1.95-2.25 Å and in the chains formed by trigonal prisms, the interionic distance A–A is ~ 2.78 Å, as calculated from the Rietveld refinement data. In the LiZnMo structure, the isolated [MoO₄]²⁻ tetrahedrons are linked by AO₆ chains creating a tunnel-like hexagonal structure, figure 4. The surrounding of the hexagonal “tunnel” consist of chains formed by the A(1) octahedrons and edge-sharing A(3) trigonal prisms, and the face-sharing A(2) octahedral polyhedrons pass through the center of this “tunnel”.

The concentration of Yb³⁺ ions in the grown crystals was determined by Energy-Dispersive X-ray (EDX) spectroscopy using an Electron Scanning Environmental Microscope (ESEM) equipped with an Inca microanalyzer (Oxford Instruments) to be 0.7 ± 0.2 at.% and 3.6 ± 0.2 at.% for the nominal doping levels of 2 and 10 at.% Yb ($N_{\text{Yb}} = 0.60$ and 3.1×10^{20} cm⁻², respectively). Thus, the segregation coefficient for the Yb³⁺ ions in LiZnMo, $K_{\text{RE}} = N_{\text{crystal}}/N_{\text{solution}} \sim 0.35 \pm 0.02$. This low value is attributed to the difference of the ionic radii for Zn²⁺ (0.74 Å for VI-fold O²⁻-coordination), Li⁺ (0.76 Å) and Yb³⁺ (0.868 Å).

3. Raman spectroscopy

The Raman spectra were measured in polarized light using a Renishaw inVia confocal Raman microscope with a x50 Leica objective. The excitation wavelength λ_{exc} was 514 nm (Ar⁺ laser) and an edge filter was used. A polished 0.7 at.% Yb:LiZnMo sample cut along the growth direction (*b*-axis) was used. The spectra corresponded to the configurations *b(aa)b*, *b(ac)b* and *b(cc)b*, see figure 5.

The Raman spectra of Yb:LiZnMo are strongly polarized. The observed Raman bands can be classified into three groups of vibrations [26]: (i) translational and rotational modes of the MoO₄ tetrahedrons and Li/Zn – O external modes at < 300 cm⁻¹; (ii) symmetric and asymmetric O – Mo – O bending vibrations at 300 – 450 cm⁻¹; (iii) Mo – O stretching modes at 750-850 cm⁻¹ (asymmetric) and at 850-1000 cm⁻¹ (symmetric). The most intense band consists of two closely located peaks centered at 898 and 912 cm⁻¹ attributed to the ν_1 mode of the [MoO₄]²⁻ tetrahedrons (non-degenerated symmetric stretching); the full width at half maximum (FWHM) of these peaks is 26 and 17 cm⁻¹, respectively.

4. Optical spectroscopy

The orthorhombic LiZnMo crystal is optically biaxial. Consequently, the optical indicatrix axes coincide with the *a*, *b*, *c* crystallographic ones [30] while their exact assignment is still unknown. In [20], the refractive index of undoped LiZnMo was measured to be ~1.97 at 579 nm and the birefringence was determined to be ~0.02.

The absorption spectra of the 0.7 at.% Yb:LiZnMo crystal were measured with polarized light ($E \parallel a, b, c$) using a Varian CARY 5000 spectrophotometer. The absorption cross-sections, σ_{abs} , were calculated as $\alpha_{\text{abs}}/N_{\text{Yb}}$, where α_{abs} is the absorption coefficient and $N_{\text{Yb}} = 0.60 \times 10^{20}$ cm⁻³ (0.7 at.%). The results are shown in figure 6(a). The Yb:LiZnMo crystal exhibits a strong anisotropy of the spectroscopic properties. The maximum $\sigma_{\text{abs}} = 11.1 \times 10^{-19}$ cm² at 972.6 nm for light polarization $E \parallel a$. The corresponding FWHM of the absorption peak is 7.3 nm. For $E \parallel b$ and $E \parallel c$, the peak σ_{abs} are lower, 5.5 and 5.1×10^{-19} cm², respectively. These values are lower than those for Yb³⁺-doped tetragonal DMos, NaLa(MoO₄)₂ (NaLaMo) and LiLa(MoO₄)₂ (LiLaMo), namely 2.1 and 1.9×10^{-20} cm² at 976 nm for $E \parallel c$, respectively [10, 31]. A broad absorption band for Yb:LiZnMo relaxes the effect of the temperature drift of a laser diode wavelength in the pumping process for the realization of a diode-pumped solid-state laser (DPSSL). Physically, it is attributed to the distortion of the crystal field due to the large difference of ionic radii for Zn²⁺ and Yb³⁺.

The luminescence spectra were measured with polarized light using a lock-in amplifier (Stanford Research Systems, model SR810), a monochromator MDR-23 and an InGaAs PIN photodiode (Hamamatsu, model G5851). The excitation was from an InGaAs laser diode emitting at 940 nm. The stimulated-emission (SE) cross-sections were calculated from the measured luminescence spectra using the Füchtbauer–Ladenburg (F-L) equation [32] adopted for biaxial crystals [33]:

$$\sigma_{\text{SE}}^{(i)}(\lambda) = \frac{\lambda^5}{8\pi n^2 \tau_{\text{rad}} c} \frac{3W_i(\lambda)}{\sum_{i=a,b,c} \int \lambda W_i(\lambda) d\lambda}. \quad (1)$$

Here, $i = a, b, c$ indicates the light polarization, $\sigma_{\text{SE}}^{(i)}$ are the SE cross-sections for the i -th polarization, λ is the light wavelength, $n = 1.93$ is the mean refractive index of the crystal at ~1 μm (as estimated from the dispersion [20]), c is the speed of light, $\tau_{\text{rad}} = 1.55$ ms is the radiative lifetime of the emitting state (the ²F_{5/2} state of Yb³⁺, see below), $W_i(\lambda)$ is the luminescence spectrum for the i -th polarization. The results are shown in figure 6(b).

The maximum $\sigma_{\text{SE}} = 8.2 \times 10^{-19}$ cm² at 982.9 nm for light polarization $E \parallel a$. However, as Yb³⁺ represents a quasi-three-level laser scheme, the laser operation is expected at longer

wavelengths than the zero-phonon-line (ZPL, $E_{ZPL} = 10176 \text{ cm}^{-1}$ (982.7 nm) for Yb:LiZnMo). In this case, the largest $\sigma_{SE} = 6.6 \times 10^{-21} \text{ cm}^2$ is observed at 1011 nm for $E \parallel b$. This is lower than for tetragonal DMos, Yb:NaLaMo and Yb:LiLaMo, $2.6 \times 10^{-20} \text{ cm}^2$ at $\sim 1000 \text{ nm}$ and $1.5 \times 10^{-20} \text{ cm}^2$ at $\sim 1011 \text{ nm}$ for $E \parallel c$, respectively [10,31].

Considering the quasi-three-level nature of the Yb³⁺ laser, the gain cross-sections, $\sigma_g = \beta\sigma_{SE} - (1 - \beta)\sigma_{abs}$, where $\beta = N_2(^2F_{5/2})/N_{Yb}$ is the inversion ratio, were calculated for the Yb:LiZnMo crystal for the high-gain light polarizations $E \parallel a$ and b , figure 7. The gain bandwidth (FWHM) is $\sim 51 \text{ nm}$ and 30 nm for the two polarizations, respectively (for $\beta = 0.3$). Such a broad gain spectra for the Yb:LiZnMo crystal make it very promising for broadly tunable lasers with a potential tuning range of $>90 \text{ nm}$ and for mode-locked lasers generating sub-100 fs pulses. The determined gain bandwidths for Yb:LiZnMo are broader than for tetragonal DMO, Yb:NaLaMo ($\sim 41 \text{ nm}$) [10].

To measure the luminescence decay, we used a ns optical parametric oscillator Lotis TII LT-2214 tuned to 972 nm as an excitation source and a monochromator MDR-12, the same photodiode (response time, $<100 \text{ ns}$) and a 500 MHz Textronix TDS-3052B digital oscilloscope as a detection system. To avoid the radiation trapping effects, the crystal sample was finely powdered and immersed in glycerin with a powder/solvent ratio varying from 10 to 70 wt.%.

The 0.7 at.% Yb-doped crystal did not show any notable dependence of the measured decay curve on the powder/solvent ratio, the typical decay curve plotted in a semi-log scale is shown in figure 8. It is clearly linear supporting the previous conclusion about a single type of site for Yb³⁺ ions and the characteristic decay time τ_{exp} is 1.55 ms. For the 3.6 at.% Yb-doped crystal, $\tau_{exp} = 1.86 \text{ ms}$ for the bulk crystal and it decreased to $\sim 1.55 \text{ ms}$ for powder/solvent ratios $< 30 \text{ wt.}\%$.

For Yb³⁺ ions, one can estimate the radiative lifetime with the modified reciprocity method adopted for biaxial crystals [34]:

$$\tau_{rad} = 8\pi n^2 c \frac{Z_2}{Z_1} \frac{3e^{-hc/kT\lambda}}{\sum_{i=a,b,c} \int \sigma_{abs}^{(i)}(\lambda) \lambda^{-4} e^{-hc/kT\lambda} d\lambda} \quad (2)$$

Here, h is the Planck constant, k is the Boltzmann constant, T is the crystal temperature (RT), and $Z_{1(2)}$ are the partition functions for the lower and upper states, respectively. The ratio Z_1/Z_2 can be determined from the Stark splitting of both multiplets. According to our low-temperature (6 K) studies employing an Oxford Instruments Ltd. cryostat (SU 12 model) with helium-gas close-cycle flow, $Z_1/Z_2 = 0.909$ for Yb:LiZnMo. This value is very close to that of another complex molybdate, trigonal Yb:K₅Bi(MoO₄)₄ (Yb:KBiMo), $Z_1/Z_2 = 0.889$ [35]. From Eq. (2), $\tau_{rad} = 1.55 \pm 0.05 \text{ ms}$ and the luminescence quantum yield $\eta_q = \tau_{exp}/\tau_{rad} > 99\%$. Such a high value is in good agreement with the large phonon energies of the host matrix, figure 5, minimizing the non-radiative relaxation. The determined τ_{rad} for Yb:LiZnMo is much longer than that for the tetragonal DMos, LiGd(MoO₄)₂ (Yb:LiGdMo) (250 μs), Yb:NaLaMo (290 μs), and Yb:LiLaMo (390 μs) [10,31,36], and slightly shorter than for trigonal Yb:KBiMo (1.93 ms) [35].

5. Conclusion

To conclude, we report on the growth, structure, Raman and optical spectroscopic characterization of a novel complex molybdate crystal – orthorhombic Yb:Li₂Zn₂(MoO₄)₃. This crystal exhibits strong anisotropy of the transition cross-sections of Yb³⁺ ions in polarized light favoring linearly polarized laser output, broad emission bands (the gain bandwidth is up to $\sim 50 \text{ nm}$) which is of interest for broadly tunable lasers at $\sim 1 \mu\text{m}$ and good energy storage capability (the lifetime of the upper laser level is $\sim 1.55 \text{ ms}$). The latter is of interest for Q-

switched lasers. Further work will focus on the laser operation with Yb:LiZnMo. For this, *c*-cut crystals are of interest as they will give access to the high-gain polarizations $E \parallel a$ and $E \parallel b$. The low solubility of Yb³⁺ ions in LiZnMo limits the available doping level (0.7 at.% Yb³⁺ for crystals of high optical quality), so further optimization of the growth conditions is necessary to achieve >3 at.% Yb³⁺-doped crystals. We believe that it can be reached by a proper control of the solute/solvent concentration and the temperature gradients in the crucible.

Acknowledgments

This work was funded by the subsidy allocated to Kazan Federal University for the state assignment in the sphere of scientific activities and Russian Government Program of Competitive Growth of Kazan Federal University. P. L. acknowledges financial support from the Government of the Russian Federation (Grant 074-U01) through ITMO Post-Doctoral Fellowship scheme. P. L. also thanks Dr. Olga Dymshits (St. Petersburg) for the XRD measurement.

References

- [1] Petrov V, Pujol M C, Mateos X, Silvestre Ò, Rivier S, Aguiló M, Solé R, Liu J, Griebner U and Díaz F 2007 *Laser & Photonics Rev.* **1** 179-212.
- [2] Cascales C et al 2006 *Phys. Rev. B* **74**174114-1-15.
- [3] Rico M, Liu J, Griebner U, Petrov V, Serrano M D, Esteban-Betegón F, Cascales C and Zaldo C 2004 *Opt. Express* **12** 5362-7.
- [4] Jacobsson B, Hellström J E, Pasiskevicius V and Laurell F 2007 *Opt. Express* **15** 1003-10.
- [5] Griebner U, Rivier S, Petrov V, Zorn M, Erbert G, Weyers M, Mateos X, Aguiló M, Massons J and Díaz F 2005 *Opt. Express* **13** 3465-70.
- [6] Liu H, Nees J and Mourou G 2001 *Opt. Lett.* **26** 1723-5.
- [7] Castellano-Hernández E, Han X, Rico M, Roso L, Cascales C and Zaldo C 2015 *Opt. Express* **23** 11135-40.
- [8] Zhao H and Major A 2013 *Opt. Express* **21** 31846-51.
- [9] Loiko P A, Xan X, Yumashev K V, Kuleshov N V, Serrano M D, Cascales C and Zaldo C 2013 *Appl. Phys. B* **111** 279-87.
- [10] Voronko Yu K, Subbotin K A, Shukshin V E, Lis D A, Ushakov S N, Popov A V and Zharikov E V 2006 *Opt. Mater.* **29** 246-52.
- [11] Pujol M C et al 2002 *Phys. Rev. B* **65** 165121-1-11.
- [12] Silvestre O et al *Opt. Express* **16** 5022-34.
- [13] Mateos X, Solé R, Gavalda Jna, Aguiló M, Massons J, Díaz F, Petrov V and Griebner U 2006 *Opt. Mat.* **28** 519-23.
- [14] Lagatsky A A, Kuleshov N V and Mikhailov V P 1999 *Opt. Commun.* **165** 71-5.
- [15] Liu J, Petrov V, Zhang H and Wang J 2007 *Appl. Phys. B* **88** 527-30.
- [16] Loiko P A, Kisel V E, Konsratuk N V, Yumashev K V, Kuleshov N V and Pavlyuk A A 2013 *Opt. Mater.* **35** 582-5.
- [17] Loiko P, Serres J M, Mateos X, Yumashev K, Yasukevich A, Petrov V, Griebner U, Aguiló M and Díaz F 2016 *Opt. Lett.* **41** 2620-3.
- [18] Pekarek S, Fiebig C, Stumpf M C, Oehler A E H, Paschke K, Erbert G, Sudmeyer T and Keller U 2010 *Opt. Express* **18** 16320-6.
- [19] Smit J P, Stair P C and Poepplmeier K R 2006 *Chem. Eur. J.* **12** 5944-53.
- [20] Bashmakova N V et al 2009 *Funct. Mater.* **16** 266-74.
- [21] Xue L, Wang Y, Lv P, Chen D, Lin Z, Liang J, Huang F and Xie Z 2009 *Cryst. Growth Design* **9** 914-20.
- [22] Trifonov V A, Pavlyuk A A, Gorbachenya K N, Yasyukevich A S and Kuleshov N V 2013 *Inorg. Mater.* **49** 517-9.
- [23] Sebastian L, Piffard Y, Shukla A K, Taulelle F and Gopalakrishnan J 2003 *J. Mater. Chem.* **13** 1797-802.

- [24] Mazur L I, Mazur M M, Pavlyuk A A and Solodovnikov S F 2010 *Inorg. Mater.* **46** 1353-8.
- [25] He X, Guan M, Zhang C, Shang T, Lian N and Yao Y 2011 *J. Alloy Compd.* **509** L341-L343.
- [26] Loiko P, Vilejshikova E V, Volokitina A A, Trifonov V A, Serres J M, Mateos X, Kuleshov N V, Yumashev K V, Baranov A V and Pavlyuk A A 2017 *J. Lumin.* doi: 10.1016/j.jlumin.2017.04.021.
- [27] Trifonov V A and Pavlyuk A A 2012 *BSU Bull. Phys. Chem.* **3** 13-7 [In Russian].
- [28] Klevtsova R F and Magarill S A 1971 *Sov. Phys. Crystallogr.* **15** 611.
- [29] Solodovnikov S F, Solodovnikova Z A, Zolotova E S, Yudanova L I, Kardash T Yu, Pavlyuk A A and Nadolinny V A 2009 *J. Solid State Chem.* **182** 1935-43.
- [30] Loiko P A and Major A 2016 *Opt. Mater. Express* **6** 2177-83.
- [31] Huang X, Lin Z, Zhang L and Wang G 2007 *J. Cryst. Growth* **306** 208-11.
- [32] Aull B F and Jenssen H P 1982 *IEEE J. Quantum Electron.* **18** 925-930.
- [33] Mateos X, Serres J M, Loiko P, Griebner U, Petrov V, Yumashev K, Aguiló M and Díaz F 2017 *J. Lumin.* **183** 391-400.
- [34] Yasyukevich A S, Shcherbitskii V G, Kisel' V É, Mandrik A V and Kuleshov N V 2004 *J. Appl. Spectr.* **71** 202-8.
- [35] Canibano H, Boulon G, Palatella L, Guyot Y, Brenier A, Voda M, Balda R and Fernandez J 2003 *J. Lumin.* **102** 318-26.
- [36] Rico M, Griebner U, Petrov V, Ortega P, Han X, Cascales C and Zaldo C 2006 *J. Opt. Soc. Am. B* **23** 1083-90.



Figure 1 Photograph of the as-grown boules of the LiZnMo crystal doped with (nominally) 2 at.% Yb; the growth direction is along the [010] axis.

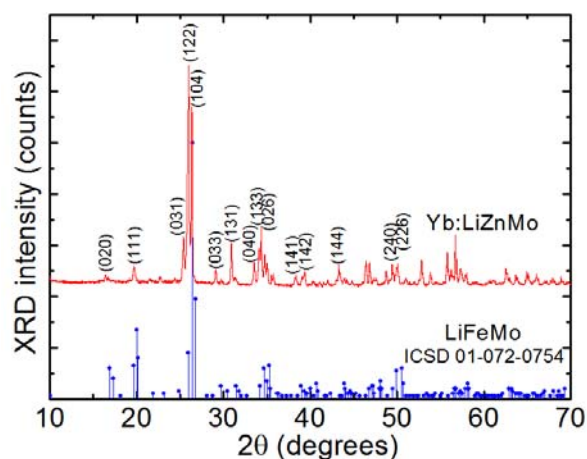


Figure 2 X-ray diffraction (XRD) pattern of a finely powdered 0.7 at.% Yb:LiZnMo crystal, the numbers indicate the Miller's indices (hkl).

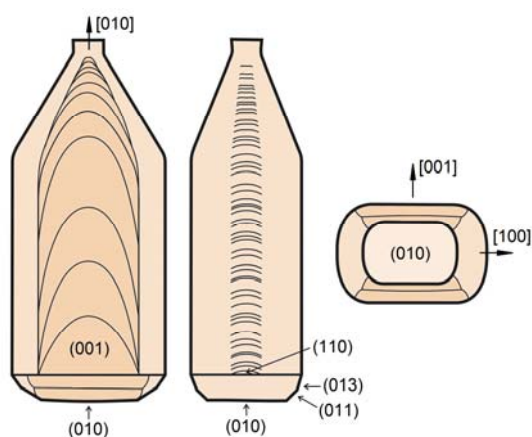


Figure 3 Habit of the as-grown 0.7 at.% Yb:LiZnMo crystal, the numbers indicate the crystallographic planes (hkl) and axes [hkl].

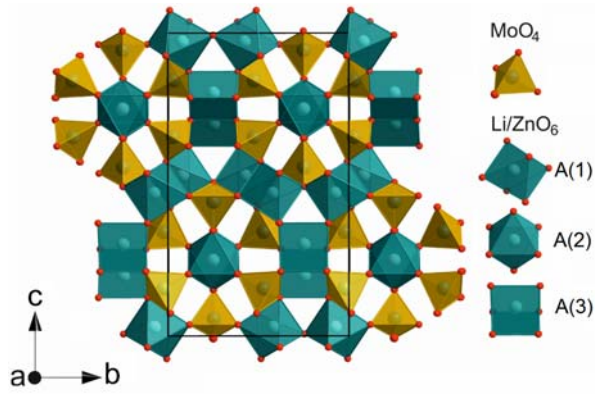


Figure 4 A fragment of the Yb:LiZnMo crystal structure in projection on the b - c plane. The Yb^{3+} ions replace the Zn^{2+} ones in the A(3) sites. Black rectangle indicates the unit-cell.

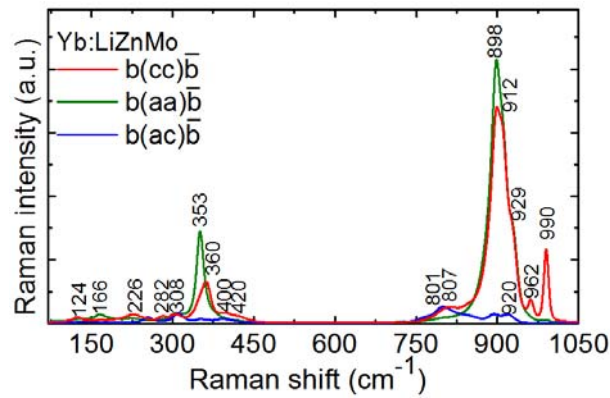


Figure 5 Polarized Raman spectra of the 0.7 at.% Yb:LiZnMo crystal for $b(xy)b$ geometry, $x, y = a$ or c . The numbers indicate the most intense Raman bands (for their complete list, refer to Table 1).

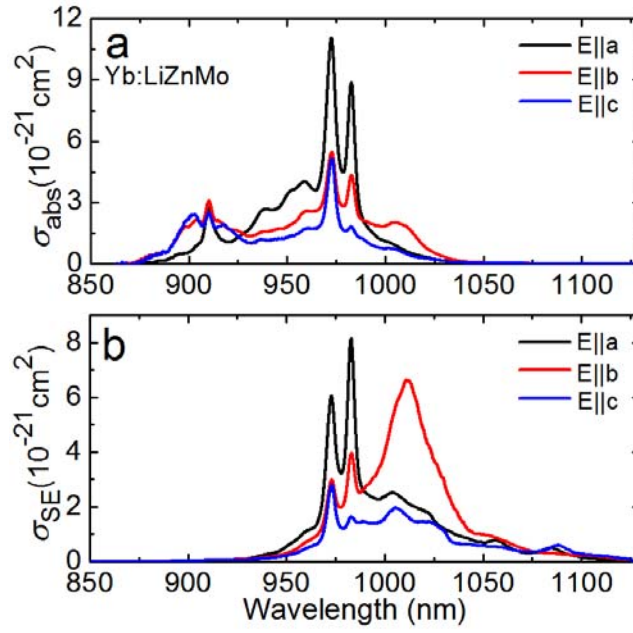


Figure 6 (a) Absorption, σ_{abs} , and (b) stimulated-emission, σ_{SE} , cross-section spectra for the 0.7 at.% Yb:LiZnMo crystal and light polarizations $E \parallel a, b, c$.

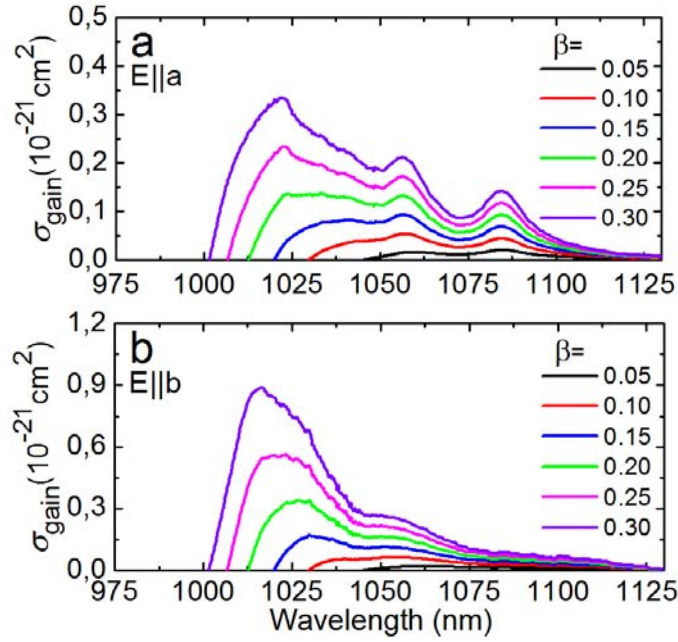


Figure 7 Gain cross-section, $\sigma_{\text{g}} = \beta\sigma_{\text{SE}} - (1 - \beta)\sigma_{\text{abs}}$, spectra for the 0.7 at.% Yb:LiZnMo crystal and light polarizations $E \parallel a$ (a) and $E \parallel b$ (b), $\beta = N_2(^2F_{5/2})/N_{\text{Yb}}$ is the inversion ratio.

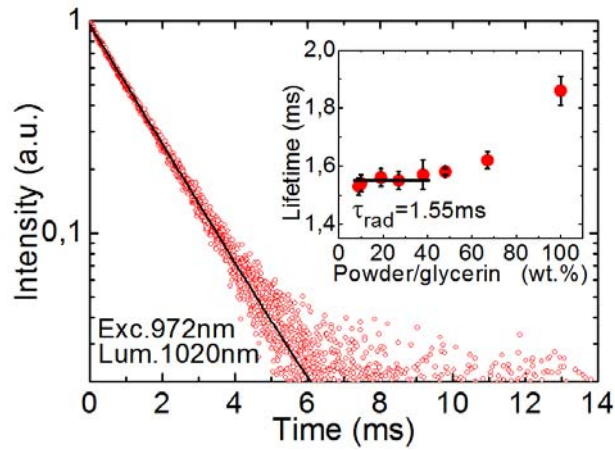


Figure 8 Luminescence decay curve for the 0.7 at.% Yb:LiZnMo crystal (*circles* – experimental data, *black line* – single-exponential fit); *inset*: dependence of the measured decay time on the powder/solution ratio for 3.6 at.% Yb:LiZnMo.